

# Characterizing Agent-Based Model Dynamics via $\varepsilon$ -Machines and Kolmogorov-Style Complexity

Roberto Garrone

*Department of Informatics, Systems and Communication (DISCo), University of Milan-Bicocca, Viale Sarca 336,, Milan, Italy*

---

## Abstract

We propose a two-level information-theoretic framework for characterizing the informational organization of Agent-Based Model (ABM) dynamics within the broader paradigm of Complex Adaptive Systems (CAS). At the macro level, a pooled  $\varepsilon$ -machine is reconstructed as a reference model summarizing the system-wide informational regime. At the micro level,  $\varepsilon$ -machines are reconstructed for each caregiver–elder dyad and variable, complemented by algorithm-agnostic Kolmogorov-style measures, including normalized LZ78 complexity and bits per symbol from lossless compression. The resulting feature set,  $\{h_\mu, C_\mu, E, \text{LZ78, bps}\}$ , enables distributional analysis, stratified comparisons, and unsupervised clustering across agents and scenarios. Empirical results show that coupling  $\varepsilon$ -machines with compression diagnostics yields a coherent picture of where predictive information resides in the caregiving ABM. Global reconstructions provide a memoryless baseline ( $L=0$  under coarse symbolizations), whereas per-dyad models reveal localized structure, particularly for *walkability* under ordinal encodings ( $m=3$ ). Compression metrics corroborate these patterns: dictionary compressors agree on algorithmic redundancy, while normalized LZ78 captures statistical novelty. Socioeconomic variables display cross-sectional heterogeneity and near-memoryless dynamics, whereas spatial interaction induces bounded temporal memory and recurrent regimes. The framework thus distinguishes *semantic organization* (predictive causation and memory) from *syntactic simplicity* (description length) and clarifies how emergence manifests at different system layers. It is demonstrated on a caregiver–elder case study with dyad-level  $\varepsilon$ -machine reconstructions and compression-based diagnostics.

*Keywords:* Agent-Based Modeling, Complex Adaptive Systems,

## 1. Introduction: Complex Adaptive Systems and ABM

Complex Adaptive Systems (CAS) provide a theoretical paradigm for describing decentralized, evolving systems driven by feedback and adaptation, while Agent-Based Modeling (ABM) operationalizes this paradigm as a computational experiment. Both perspectives emphasize emergence, heterogeneity, and nonlinearity as core drivers of complex social and ecological dynamics. Integrating CAS theory with ABM practice enables researchers to link micro-level rules with macro-level phenomena and to explore resilience, innovation, and systemic sustainability *in silico* [1, 2, 3, 4].

A CAS can be conceptualized as a network of interacting and interdependent components whose local behaviors collectively generate emergent, system-level patterns that are not reducible to the attributes of individual elements. Within such systems, agents adapt to both environmental conditions and the evolving behavior of others, producing feedback loops that continually reshape the system’s structure and dynamics [1, 5]. The hallmark properties of CAS—nonlinearity, feedback, adaptation, and emergence—explain why even simple local rules can yield diverse macroscopic outcomes [6, 4, 2]. As emphasized by Bonabeau [2], global structure “emerges” from localized rules rather than centralized design, creating recursive micro–macro feedback and path dependence [7].

ABM provides a computational framework for representing and analyzing the mechanisms underlying complex adaptive behavior. In ABM, a system is represented as a collection of autonomous, heterogeneous agents—each with states, goals, and behavioral rules—interacting within a shared environment [3, 8]. Through repeated interactions, these agents produce emergent macro-level dynamics that can be analyzed to understand how collective behavior arises from individual decisions. ABM adopts a generative epistemology: it seeks to “grow” phenomena from micro-level mechanisms rather than impose top-down equations [9]. This makes it a natural complement to CAS theory, capable of exploring how adaptation, feedback, and heterogeneity shape system evolution [4, 2]. Conceptually, CAS defines the phenomenon, while ABM provides the method for its exploration [8, 2, 4].

## 2. Computational Mechanics for ABM: $\varepsilon$ -Machines

The application of  $\varepsilon$ -machine reconstruction to Agent-Based Modeling (ABM) remains uncommon, yet it is conceptually well grounded within the theory of information processing in complex systems. Originally developed in nonlinear and symbolic dynamics [10, 11], the  $\varepsilon$ -machine provides the minimal unifilar model that partitions past observation histories into sets—called *causal states*—that yield identical conditional distributions over possible futures [12]. Formally, if two pasts  $x_{:t}$  and  $x'_{:t}$  satisfy

$$\mathbb{P}(X_{t:\infty} | X_{:t} = x_{:t}) = \mathbb{P}(X_{t:\infty} | X_{:t} = x'_{:t}), \quad (1)$$

they belong to the same causal state. The  $\varepsilon$ -machine thus defines the minimal predictive architecture of the process, specifying how information from the past is stored and used to generate the future.

Three canonical quantities summarize its informational organization: the *entropy rate*  $h_\mu$  (average unpredictability per symbol), the *statistical complexity*  $C_\mu$  (information stored in the causal-state distribution), and the *excess entropy*  $E$  (shared information between past and future). In concise form:

$$h_\mu = H[X_t | X_{:t}], \quad (2)$$

$$C_\mu = H[\mathcal{S}], \quad (3)$$

$$E = I[X_{:t}; X_{t:\infty}], \quad (4)$$

where  $H[\cdot]$  and  $I[\cdot; \cdot]$  denote Shannon entropy and mutual information, respectively, and  $\mathcal{S}$  is the causal-state random variable. These quantities capture how much information a process generates, stores, and transmits over time, thereby distinguishing structured dynamics from mere randomness.

In the context of ABMs,  $\varepsilon$ -machines provide a principled means to extract and quantify the system’s intrinsic computation—the transformation of past information into future behavior. Here, causal states may correspond to recurrent behavioral regimes, coordination cycles, or macro-level feedback patterns that emerge from agent interactions. Unlike scalar measures such as entropy or mutual information alone, the  $\varepsilon$ -machine reconstructs the minimal predictive model: it reveals the architecture of information storage and flow that governs the system’s evolution. This makes it particularly suited

to studying adaptive or path-dependent ABM dynamics, where emergent regularities coexist with stochastic fluctuations. In contrast, Kolmogorov–Solomonoff–Chaitin complexity formalizes the descriptive compressibility of a sequence as the length of the shortest program that can reproduce it on a universal Turing machine [16]. Because true Kolmogorov complexity is non-computable, compression-based estimators such as Lempel–Ziv provide practical proxies [13].

The achieved compressed size reflects the regularity and redundancy of the sequence. A general compression-based complexity proxy is defined as:

$$C_{\text{comp}} = \frac{8 S_{\text{comp}}}{n}, \quad (5)$$

where  $S_{\text{comp}}$  is the compressed file size in bytes and  $n$  is the number of symbols in the input sequence. The factor 8 converts bytes to bits, since 1 byte = 8 bits. This expression yields a value in bits per symbol, providing a dimensionless estimate of Kolmogorov complexity that is directly comparable to the entropy rate ( $h_\mu$ ). Compression libraries such as `lzma`, `bz2`, and `gzip` report sizes in bytes, making this normalization necessary for consistency with information-theoretic measures. Lower values of  $C_{\text{comp}}$  indicate greater compressibility and structural regularity, while higher values reflect increased algorithmic novelty and unpredictability.

Both perspectives are complementary: the  $\varepsilon$ -machine captures semantic organization and predictive structure—the causal organization by which the system encodes, stores, and utilizes information to generate future states—whereas compression-based metrics capture syntactic simplicity, or the descriptive regularity of the system’s observable output.

### 3. Proposed Framework for Analyzing ABM Dynamics

#### 3.1. Global $\varepsilon$ -Machine as System-Level Reference

A single  $\varepsilon$ -machine is reconstructed from a pooled, symbolized time series (e.g., `efforts`) using quantile-based discretization. The optimal Markov order is selected by the Bayesian Information Criterion (BIC) up to  $L_{\text{max}}$ , and histories are clustered by  $L_1$  distance to obtain causal states. The resulting  $(h_\mu, C_\mu, E)$  summarize the system-wide informational regime. When BIC selects  $L = 0$ , the pooled process behaves approximately memoryless under the chosen resolution, providing a succinct contextual baseline for finer-grained analyses.

### 3.2. Per-Dyad, Multi-Variable $\varepsilon$ -Machines and Algorithmic Proxies

Each dyad is treated as an independent stochastic process. For each variable—`efforts`, `wkb`, `hrsncared` (with a hurdle at zero), and binary `overwhelmed`—we reconstruct one  $\varepsilon$ -machine per dyad, obtaining  $\{h_\mu^{(i,v)}, C_\mu^{(i,v)}, E^{(i,v)}\}$  and defining a *complexity signature*. These measures are complemented by algorithm-agnostic proxies: (i) normalized LZ78 complexity, and (ii) bits per symbol from lossless compression (LZMA, BZ2, GZIP). These proxies remain informative even when  $\varepsilon$ -machines collapse to trivial structures and provide clusterable feature sets for comparative and multivariate analysis.

### 3.3. Comparative Overview of LZMA, BZ2, and GZIP Compression Algorithms

The compression algorithms LZMA, BZ2, and GZIP all originate from the *Lempel–Ziv family* of lossless compression schemes, yet they differ substantially in their modeling depth, computational efficiency, and ability to detect long-range dependencies. When applied as proxies for Kolmogorov complexity, these differences translate into distinct sensitivities to structural regularity in symbolic sequences produced by agent-based models.

LZMA (Lempel–Ziv–Markov chain algorithm) employs range coding and Markov-chain modeling to capture both local and distant symbol dependencies. It generally achieves the highest compression ratios among the three methods, albeit at a significant computational cost. This makes it particularly appropriate for sequences with complex or hierarchical patterns, where predictive dependencies extend over long horizons. Its precision, however, comes at the expense of speed and memory consumption, which may be nontrivial for large-scale simulations.

BZ2, based on the Burrows–Wheeler transform, operates through block sorting followed by move-to-front and Huffman encoding. It provides an effective compromise between compression strength and computational cost, being capable of detecting medium-range regularities without the substantial resource demands of LZMA. Its performance tends to be stable across moderately redundant or quasi-periodic data, although it becomes less efficient for short or highly stochastic sequences.

GZIP, which implements the DEFLATE algorithm combining LZ77 windowed matching with Huffman coding, emphasizes processing speed and portability. It achieves lower compression ratios but operates efficiently even

on small data fragments. Because of its shallow dictionary window, GZIP predominantly captures short-term correlations, making it a fast but coarse estimator of descriptive regularity.

When interpreted within a complexity-theoretic framework, these algorithms offer complementary perspectives. The normalized measure is defined as:

$$C_{\text{comp}} = \frac{8 S_{\text{comp}}}{n}, \quad (6)$$

where  $S_{\text{comp}}$  is the compressed file size in bytes and  $n$  is the sequence length. This expression quantifies the bits per symbol required to encode the data. LZMA thus approximates long-range structural predictability, BZ2 captures intermediate regularities, and GZIP provides an estimate dominated by local redundancy. Using multiple codecs within the same analytical framework yields a *multi-scale assessment* of algorithmic regularity—analogous to evaluating informational structure at different temporal or spatial resolutions in entropy-based analyses.

#### 3.4. Hierarchical Scopes and Visualization

Metrics are reported at the dyad (micro) and global (macro) levels. The framework also supports meso-level aggregation (by stage, disability, or other strata), enabling future cross-stratum comparisons that summarize heterogeneity across subgroups. For dissemination, we include (i) distributions and heatmaps of  $\{h_{\mu}, C_{\mu}, E, \text{LZ78}, \text{bps}\}$  by variable and dyad, and (ii) a concise global  $\varepsilon$ -machine diagram as a macro-level reference. This multi-scale representation preserves heterogeneity while providing an interpretable, system-wide informational baseline.

### 4. System Level $\varepsilon$ -machine Reconstruction

In the context of agent-based models (ABMs),  $\varepsilon$ -machines provide a principled means to extract and quantify a system’s intrinsic computation—the transformation of past information into future behavior. Here, causal states may correspond to recurrent behavioral regimes, coordination cycles, or macro-level feedback patterns that emerge from agent interactions. Unlike scalar measures such as entropy or mutual information alone, the  $\varepsilon$ -machine reconstructs the *minimal predictive model*: it reveals the architecture of information storage and flow that governs the system’s evolution. This makes it

particularly suited to studying adaptive or path-dependent ABM dynamics, where emergent regularities coexist with stochastic fluctuations.

The  $\varepsilon$ -machine provides the minimal unifilar model that partitions past observation histories into sets—called causal states—that yield identical conditional distributions over possible futures. Formally, if two pasts  $(x_{:t})$  and  $(x'_{:t})$  satisfy

$$\mathbb{P}(X_{t:\infty} | X_{:t} = x_{:t}) = \mathbb{P}(X_{t:\infty} | X_{:t} = x'_{:t}), \quad (7)$$

then they belong to the same causal state. The  $\varepsilon$ -machine thus defines the minimal predictive architecture of the process, specifying how information from the past is stored and used to generate the future.

Three canonical quantities summarize its informational organization: the entropy rate  $h_\mu$  (average unpredictability per symbol), the statistical complexity  $C_\mu$  (information stored in the causal-state distribution), and the excess entropy  $E$  (shared information between past and future). In concise form:

$$h_\mu = H[X_t | X_{:t}], \quad (8)$$

$$C_\mu = H[\mathcal{S}], \quad (9)$$

$$E = I[X_{:t}; X_{t:\infty}], \quad (10)$$

where  $H[\cdot]$  and  $I[\cdot; \cdot]$  denote Shannon entropy and mutual information, respectively, and  $\mathcal{S}$  is the causal-state random variable. These quantities capture how much information a process generates, stores, and transmits over time, thereby distinguishing structured dynamics from mere randomness.

Accurate estimation of these quantities, however, critically depends on how continuous simulation outputs are represented as discrete symbolic sequences. Symbolization—the transformation of numeric or multidimensional trajectories into finite alphabets—acts as the analytical lens through which temporal organization becomes observable. An appropriate scheme determines which variations are treated as equivalent and which are preserved as meaningful distinctions. Poorly chosen symbolizations can obscure dependencies by merging distinct states or, conversely, fabricate structure by discretizing noise into artificial categories. In agent-based simulations, this step is particularly delicate because variables differ in scale and generative

mechanism: spatial indicators such as *walkability* exhibit smooth continuity and feedback, requiring ordinal or rank-based encodings that preserve relative change, whereas socioeconomic measures like *caregiver effort* or *hours not cared* vary primarily across agents and are better discretized using quantile or hurdle-mixture schemes. Symbolization thus defines the *effective alphabet* and the *grain of observation*, balancing detail and parsimony. Finer encodings may inflate entropy and complexity through over-partitioning, while coarser ones suppress correlations and underestimate structure. Beyond its technical role, symbolization is a modeling decision: it specifies the mapping between the simulated micro-dynamics and the informational architecture that  $\varepsilon$ -machines can reveal.

#### 4.1. $\varepsilon$ -Machine Reconstruction and Entropy Estimation Pipeline

The pipeline transforms a univariate symbolic series into a minimal predictive-state representation, evaluates both causal and block-entropy-based complexity metrics, and produces graphical and tabular outputs for subsequent analysis. Given an input sequence of discrete symbols  $\mathbf{s} = (s_1, s_2, \dots, s_n)$  with  $s_t \in \{0, \dots, A-1\}$ , the alphabet size  $A$  is inferred as  $A = \max(\mathbf{s}) + 1$  if not provided.

##### 4.1.1. $\varepsilon$ -Machine Reconstruction

The input sequence of integer symbols is first normalized, and the alphabet size is inferred from the data unless explicitly specified. The main reconstruction step builds a probabilistic, unifilar state model. Within this stage, the optimal Markov order  $L^*$  is determined by minimizing the Bayesian Information Criterion (BIC) across candidate orders  $L = 0, \dots, L_{\max}$ .

For each candidate order  $L$ , the empirical next-symbol probabilities are defined as:

$$\hat{P}(a | h) = \frac{N(h, a)}{N(h)}, \quad N(h, a) = |\{t : s_{t-L:t-1} = h, s_t = a\}|, \quad (11)$$

where  $h$  denotes a history of length  $L$ . The log-likelihood and Bayesian Information Criterion are then given by:

$$\log \mathcal{L}_L = \sum_h \sum_a N(h, a) \log \hat{P}(a | h), \quad (12)$$

$$\text{BIC}(L) = -2 \log \mathcal{L}_L + k_L \log N_{\text{eff}}, \quad (13)$$

where  $k_L$  is the number of free parameters and  $N_{\text{eff}} \approx n - 1 - L$ . The order  $L^*$  minimizing  $\text{BIC}(L)$  is then selected as the optimal Markov order.

#### 4.1.2. Predictive Distributions and History Clustering

For the selected order, predictive conditional distributions  $P(a_{t+1} | a_{t-L:t})$  are estimated for all histories observed with sufficient frequency. Histories with statistically similar predictive distributions (as measured by their  $L_1$  distance) are clustered to form equivalence classes representing causal states.

For each observed history  $h$ , we estimate:

$$P(a | h) = \frac{N(h, a)}{N(h)}, \quad a \in \{0, \dots, A-1\}, \quad (14)$$

where  $N(h, a)$  is the joint count of occurrences of history  $h$  followed by symbol  $a$ , and  $N(h)$  is the total count of  $h$ . Histories observed fewer than a threshold count are discarded to suppress noise. Two histories  $h$  and  $h'$  belong to the same causal state if their  $L_1$  distance satisfies

$$\|P(\cdot | h) - P(\cdot | h')\|_1 \leq \text{tol}. \quad (15)$$

Each causal state  $s$  thus represents a cluster of statistically equivalent histories  $C_s$ . The mean emission distribution for each state is computed as

$$P_{\text{emit}}(a | s) = \frac{1}{|C_s|} \sum_{h \in C_s} P(a | h), \quad (16)$$

defaulting to a uniform vector if no histories are present.

#### 4.1.3. Unifilar Transitions and Stationary Distribution

A *unifilar transition structure* is a type of state–transition topology used in computational mechanics and predictive-state models (such as  $\varepsilon$ -machines), where each state–symbol pair uniquely determines the next state. A transition function  $T(s, a) = s'$  is constructed by majority rule over history shifts, producing a deterministic mapping between states and emitted symbols.

For each history  $h \in C_s$  and symbol  $a$ , the shifted context is defined as

$$h' = \text{shift}_L(h, a), \quad (17)$$

and the next state  $s'$  is chosen as the most frequent state reached by these shifts. The corresponding state-transition matrix  $M$  is defined as

$$M_{ij} = \sum_a P_{\text{emit}}(a \mid s_i) \mathbf{1}\{T(s_i, a) = s_j\}, \quad (18)$$

and it is normalized row-wise to ensure stochasticity. The stationary distribution  $\pi$  satisfies

$$\pi = \pi M, \quad \pi^{(t+1)} = \pi^{(t)} M, \quad \|\pi^{(t+1)} - \pi^{(t)}\|_1 < \text{tol}. \quad (19)$$

States with similar emission distributions can optionally be merged using a Jensen–Shannon divergence threshold, regularizing the model by removing redundant predictive structures.

#### 4.1.4. Optional State Merging by Jensen–Shannon Divergence

To regularize over-fragmented models, states with similar emissions are merged when

$$\text{JS}(P_{\text{emit}}(\cdot \mid s), P_{\text{emit}}(\cdot \mid s')) \leq \tau_{\text{JS}}, \quad (20)$$

where  $\text{JS}(P, Q)$  is the Jensen–Shannon divergence and  $\tau_{\text{JS}}$  controls the merging threshold. The divergence is defined as

$$\text{JS}(p, q) = \frac{1}{2} D_{\text{KL}}(p \parallel m) + \frac{1}{2} D_{\text{KL}}(q \parallel m), \quad m = \frac{1}{2}(p + q), \quad (21)$$

and after merging, the stationary distribution  $\pi$  is recomputed.

#### 4.1.5. Information-Theoretic Quantities

From the reconstructed  $\varepsilon$ -machine, the following information-theoretic quantities are derived.

*Entropy rate..*

$$h_\mu = \sum_s \pi_s H(P_{\text{emit}}(\cdot \mid s)), \quad H(p) = - \sum_i p_i \log_2 p_i, \quad (22)$$

quantifying the average unpredictability of symbol generation.

*Statistical complexity..*

$$C_\mu = H(\pi) = - \sum_s \pi_s \log_2 \pi_s, \quad (23)$$

measuring the information stored in the stationary-state distribution.

*Predictive information proxy.* Let

$$P_{\text{next}} = \sum_s \pi_s P_{\text{emit}}(\cdot | s), \quad H_{\text{next}} = H(P_{\text{next}}), \quad (24)$$

then

$$E_{\text{proxy}} = \max(H_{\text{next}} - h_\mu, 0), \quad (25)$$

which approximates the system's excess entropy, where  $H_{\text{next}}$  is the entropy of the one-step mixture distribution.

#### 4.1.6. Finite-Block Entropy and Excess Entropy

An independent estimate of the entropy rate and excess entropy is computed via finite-block entropies up to order  $L_{\text{max}}$ . For each block length  $L$ , the empirical entropy  $H_L$  is estimated using a plug-in method with mild smoothing. Asymptotic values are extrapolated as

$$h_\mu^{(\text{block})} \approx H_L - H_{L-1}, \quad E^{(\text{block})} \approx H_L - L h_\mu^{(\text{block})}. \quad (26)$$

For observed  $L$ -blocks  $b \in \mathcal{B}^L$  with counts  $N(b)$  and total  $N = \sum_b N(b)$ , smoothed probabilities are estimated as

$$\hat{P}(b) = \frac{N(b) + 1}{N + |\mathcal{B}^L|}. \quad (27)$$

The block entropy is computed as

$$H_L = - \sum_b \hat{P}(b) \log_2 \hat{P}(b), \quad (28)$$

and block-based estimates are refined by averaging the last three increments of  $H_L - H_{L-1}$ :

$$h_\mu^{(\text{block})} = \text{mean} \left[ H_L - H_{L-1} \right]_{L_{\text{max}}-2}^{L_{\text{max}}}, \quad E^{(\text{block})} = \max \left( H_{L_{\text{max}}} - L_{\text{max}} h_\mu^{(\text{block})}, 0 \right). \quad (29)$$

#### 4.1.7. Visualization and Data Export

Finally, the pipeline generates the following visual and tabular artifacts:

- (i) a time-series plot of the input symbols;

- (ii) a bar plot of stationary-state probabilities;
- (iii) a transition graph representing the reconstructed  $\varepsilon$ -machine;
- (iv) JSON and CSV exports describing states, emissions, and transitions;  
and
- (v) a table of BIC scores across candidate Markov orders.

The pipeline returns the chosen order  $L^*$ , the number of causal states  $|S|$ , the entropy rate  $h_\mu$ , statistical complexity  $C_\mu$ , predictive information proxy  $E_{\text{proxy}}$ , block-based estimates  $(h_\mu^{(\text{block})}, E^{(\text{block})})$ , and file paths for all generated visual and tabular artifacts.

#### 4.2. Symbolization and Discretization Pipeline

This pipeline provides a unified framework for transforming continuous variables into discrete symbolic representations. It supports both *data-driven* (quantile, Jenks, Gaussian mixture, vector quantization) and *rule-based* (fixed, policy, winsorized) discretizations. The design is modular, with each transformation stage isolated and equipped with fallback procedures to ensure robustness under degenerate or ill-conditioned input data.

Let the numeric series be denoted by

$$\mathbf{x} = (x_1, \dots, x_n)^\top \in \mathbb{R}^n. \quad (30)$$

A binning scheme with  $k$  bins is defined by the ordered set of edges

$$\mathbf{e} = (e_0, \dots, e_k), \quad e_0 < \dots < e_k. \quad (31)$$

Each observation is assigned to a discrete label (symbol) according to

$$\ell(x_i; \mathbf{e}) = \min \left\{ j \in \{0, \dots, k-1\} : e_j \leq x_i < e_{j+1} \right\}. \quad (32)$$

The alphabet size is  $A = k$  (or fewer if bins are empty). Unless otherwise specified, bins are left-closed and right-open,  $[e_j, e_{j+1})$ . Ties and non-finite values are handled by small perturbations or exclusion before computing quantiles or class boundaries.

#### 4.2.1. Discretization Methods

Each of the methods described below produces a label vector  $\ell$ , an edge set  $\mathbf{e}$  (if applicable), and the alphabet size  $A$ . All methods follow the same high-level transformation sequence:

Input series  $\rightarrow$  [optional winsorization]  $\rightarrow$  edge computation  $\rightarrow$   
 digitization  $\rightarrow$  symbolic labeling  $\rightarrow$  output (labels, edges,  
 alphabet size)

Fallback mechanisms ensure stability: Jenks  $\rightarrow$  K-Means  $\rightarrow$  quantiles for class breaks, and default clipping to small perturbations when numerical degeneracy occurs.

1. *Quantile Bins.* Let  $Q(p)$  denote the empirical quantile of  $\{x_i\}$  at cumulative probability  $p$ . Define bin edges as

$$e_j = Q\left(\frac{j}{k}\right), \quad j = 0, \dots, k. \quad (33)$$

After enforcing monotonicity, assign labels  $\ell_i = \ell(x_i; \mathbf{e})$ . Alphabet size:  $A = k$ .

2. *Fixed or Policy-Fixed Edges.* Given explicit user-supplied cutpoints  $e_0 < e_1 < \dots < e_k$ , assign labels via  $\ell_i = \ell(x_i; \mathbf{e})$ . Alphabet size:  $A = k$ .

3. *Winsorized Equal-Width.* Using parameters  $p_{\text{low}}$  and  $p_{\text{high}}$ , compute

$$\ell = Q(p_{\text{low}}), \quad h = Q(p_{\text{high}}), \quad (34)$$

then clip as in Section 4.2.2. Edges are constructed as

$$e_j = \ell + \frac{j}{k}(h - \ell), \quad j = 0, \dots, k. \quad (35)$$

Alphabet size:  $A = k$ .

4. *Jenks Natural Breaks.* Use edges  $\mathbf{e}^*$  obtained from the Jenks optimization in Section 4.2.2. Assign labels  $\ell_i = \ell(x_i; \mathbf{e}^*)$  and set alphabet size  $A = k$ .

5. *Hurdle + Gaussian Mixture Model.* Nonpositive values form a separate bin ( $\ell_i = 0$  if  $x_i \leq 0$ ). For the positive subset  $X^+ = \{x_i > 0\}$ , fit Gaussian mixtures of varying component count  $m$ :

$$f(x; \theta_m) = \sum_{c=1}^m \pi_c \mathcal{N}(x \mid \mu_c, \sigma_c^2). \quad (36)$$

Select the optimal  $\hat{m}$  by minimizing the Bayesian Information Criterion (BIC; [14]):

$$\text{BIC}(m) = -2 \sum_{x \in X^+} \log f(x; \theta_m) + p_m \log |X^+|. \quad (37)$$

Assign each positive value to its maximum-posterior component index,

$$\tilde{\ell}(x) = \arg \max_c \pi_c \mathcal{N}(x \mid \mu_c, \sigma_c^2), \quad (38)$$

and shift labels by one to preserve the zero bin:

$$\ell(x) = \begin{cases} 0, & x \leq 0, \\ \tilde{\ell}(x) + 1, & x > 0. \end{cases} \quad (39)$$

Alphabet size:  $A = \hat{m} + 1$ .

6. *Ordinal Patterns.* For an order parameter  $m$ , construct sliding windows

$$\mathbf{w}_t = (x_{t-m+1}, \dots, x_t). \quad (40)$$

Let  $\pi_t$  be the permutation that sorts  $\mathbf{w}_t$  increasingly. Encode  $\pi_t$  into an integer index using the Lehmer code:

$$c_{t,i} = \#\{j > i : \pi_t(j) < \pi_t(i)\}, \quad \text{idx}(\pi_t) = \sum_{i=1}^m c_{t,i} (m-i)!. \quad (41)$$

Set  $\ell_t = \text{idx}(\pi_t)$  and pad the first  $(m-1)$  indices. Alphabet size:  $A = m!$ .

7. *Lagged Vector Quantization..* For lag order  $m$ , build lagged vectors

$$\mathbf{y}_t = (x_{t-m+1}, \dots, x_t)^\top, \quad t = m, \dots, n. \quad (42)$$

Optionally standardize as

$$\mathbf{z}_t = (\mathbf{y}_t - \hat{\boldsymbol{\mu}})/\hat{\sigma}, \quad (43)$$

(elementwise). Apply  $k_{\text{VQ}}$ -means clustering to minimize

$$\sum_{t=m}^n \min_j \|\mathbf{z}_t - \mathbf{c}_j\|_2^2. \quad (44)$$

Assign each vector to its nearest centroid:

$$\ell_t = \arg \min_j \|\mathbf{z}_t - \mathbf{c}_j\|_2^2. \quad (45)$$

Pad the first  $(m-1)$  samples with  $\ell_m$ . Alphabet size:  $A = k_{\text{VQ}}$ .

#### 4.2.2. Binning, Digitization, and Label Formation

Discrete labels are assigned from predefined boundaries (digitization), generating bin edges through equal-width or Jenks optimization, and optionally preprocessing data by clipping extreme values (winsorization).

*Digitization..* Given edges  $\mathbf{e}$ , integer labels are computed as

$$\ell_i = \sum_{j=1}^{k-1} \mathbb{I}\{x_i \geq e_j\}, \quad i = 1, \dots, n. \quad (46)$$

*Equal-Width Edges..* For given lower and upper endpoints  $\ell = \min_i x_i$  and  $h = \max_i x_i$  (optionally provided), define  $k$  equal-width intervals with edges

$$e_j = \ell + \frac{j}{k}(h - \ell), \quad j = 0, \dots, k. \quad (47)$$

*Jenks Natural Breaks..* Jenks natural breaks [15] minimize the within-class sum of squares:

$$\mathcal{J}(\mathbf{e}) = \sum_{c=1}^k \sum_{x_i \in C_c} (x_i - \bar{x}_{C_c})^2, \quad (48)$$

where  $\bar{x}_{C_c}$  is the class mean. The objective is equivalent to maximizing the goodness-of-variance-fit (GVF):

$$\text{GVF} = 1 - \frac{\sum_{c=1}^k \sum_{x_i \in C_c} (x_i - \bar{x}_{C_c})^2}{\sum_{i=1}^n (x_i - \bar{x})^2}, \quad \bar{x} = \frac{1}{n} \sum_i x_i. \quad (49)$$

*Winsorization..* Given probabilities  $p_{\text{low}}$  and  $p_{\text{high}}$ , define the lower and upper quantile thresholds as

$$\ell = Q(p_{\text{low}}), \quad h = Q(p_{\text{high}}), \quad (50)$$

where  $Q(p)$  is the empirical quantile function of  $\mathbf{x}$ . Each value is clipped to this interval as

$$x_i^{\text{win}} = \min\{\max\{x_i, \ell\}, h\}. \quad (51)$$

The function returns  $(\mathbf{x}^{\text{win}}, \ell, h)$ .

## 5. Case Study Outline: Caregiver–Elder Dyads

Each record in the dataset corresponds to a distinct access event by a caregiver–elder dyad at a given simulation tick. The composite key (`id_caregiver`, `tick`, `day`, `hour`) uniquely identifies observations. For each dyad  $i$ , we consider the multivariate series

$$X_t^{(i)} = \{\text{efforts}, \text{wkb}, \text{hrsncared}, \text{overwhelmed}, \dots\}_{i,t}. \quad (52)$$

Sequences are discretized via quantiles (with a hurdle at zero for `hrsncared`) and analyzed per variable. Contextual covariates (e.g., age, mobility, disability) are reserved for stratification. The dual analysis yields (a) dyad-level  $\varepsilon$ -machine measures and (b) algorithmic complexity proxies, enabling stratified comparisons (mobility, occupation, stage) and cohort-level clustering.

The initial  $\varepsilon$ -machine reconstructions performed with simple *quantile-based* symbolization ( $k = 5$ ) illustrate how the discretization of continuous data can decisively shape the inferred informational structure. Under this scheme, all three variables—*efforts*, *walkability* (`wkb`), and *hours not cared* (`hrsncared`)—collapsed into trivial  $\varepsilon$ -machines, each with a single causal state ( $L = 0$ ,  $C_\mu = 0$ ) and no measurable predictive information ( $E_{\text{proxy}} = 0$ ). Although entropy rates remained nonzero ( $h_\mu \approx 1.37\text{--}2.32$  bits per symbol), these values merely reflected random variation rather than structured dependence.

At first glance, one might conclude that the simulated system is entirely memoryless. However, such an interpretation would conflate a *true absence of dynamics* with the *failure of the symbolization* to capture them. The discrepancy between the  $\varepsilon$ -machine outcomes ( $E_{\text{proxy}} = 0$ ) and the block-entropy estimates ( $E_{\text{block}} \approx 2.3\text{--}2.9$  bits for *wkb* and *hrsncared*) already signals a deeper issue: the symbolization scheme is generating artificial long-range correlations while erasing short-range organization. This occurs because quantile binning partitions values according to their rank in the distribution, ignoring the temporal geometry of transitions between them. The resulting sequences treat adjacent values that belong to different bins as abrupt categorical changes, even when the underlying process evolves smoothly. In such conditions, entropy grows, but the algorithm cannot infer stable predictive states, producing an apparent paradox of *high randomness but no structure*.

From a methodological standpoint, this demonstrates why symbolization cannot be regarded as a neutral preprocessing step. The quantile scheme was adequate for *efforts*, whose variability is driven primarily by cross-sectional attributes (income and elder ability) rather than by temporal feedback. In that case, the absence of causal states corresponds to genuine statistical independence. Yet for *walkability* and *hours not cared*, the same discretization distorted the data-generating process: it produced  $\varepsilon$ -machines that appeared memoryless despite substantive reasons to expect autocorrelation—spatial continuity in the former and dependency on caregiving load in the latter. In both cases, the failure lies not in the reconstruction algorithm but in the representation of the signal.

The broader implication is that symbolization defines the effective topology of information available for analysis. A discretization that partitions data by frequency but disregards temporal or contextual continuity will obscure any process that encodes information in the *ordering* of observations rather than in their *amplitude*. This is particularly relevant for agent-based simulations, where variables differ not only in magnitude but also in the nature of their dependence on agents' interactions and the environment. Spatially continuous quantities, such as *walkability*, require symbolizations that preserve directional information (e.g., ordinal patterns), whereas zero-inflated behavioral measures, such as *hours not cared*, are better served by hybrid schemes that explicitly distinguish between structural zeros and positive variability (e.g., Hurdle-GMM encodings).

In information-theoretic terms, symbolization defines the mapping from the continuous dynamics of the model to the discrete alphabet used for estimating entropy and reconstructing causal states. Coarse symbolization merges distinct regimes into single symbols, suppressing predictive information and underestimating complexity; excessively fine symbolization fragments the process, producing spurious states and inflated entropy. The objective, therefore, is to identify a symbolization that stabilizes the predictive information ( $E_{\text{proxy}}$ ) while minimizing unnecessary state proliferation. In the present analysis, the quantile-based scheme failed to meet this criterion, yielding statistically inconsistent estimates across methods and masking potential dependencies that emerge only under more semantically appropriate encodings.

## 6. Case Study Results

### 6.1. Global $\varepsilon$ -Machine

The symbolic reconstruction of time series derived from the *efforts*, *hours not cared*, and *walkability* variables provides complementary insights into the internal organization of the simulated caregiving system. Although these three indicators are jointly produced by the same set of agents, they differ markedly in the degree of temporal structure and informational complexity they encode. By combining  $\varepsilon$ -machine reconstruction with block-entropy estimation, it becomes possible to distinguish between variables that are primarily *distributional*—reflecting cross-sectional variation among agents—and those that exhibit *temporal coherence*, that is, recurrent configurations of states and feedback across simulation steps.

For the caregiver effort variable, the  $\varepsilon$ -machine collapses into a single causal state with no measurable statistical complexity ( $C_\mu = 0$ ) and a moderate entropy rate ( $h_\mu \approx 1.37$ ). This outcome is consistent with a process that fluctuates randomly around fixed socioeconomic constraints. In the model, caregiving effort is largely determined by the dyad’s income and the elder’s capacity to perform activities of daily living (ADL), both of which are static attributes rather than evolving states. Consequently, each observed episode of effort represents an independent draw from a stationary distribution rather than a temporally conditioned decision sequence. The absence of predictive information ( $E_{\text{proxy}} = 0$ ) confirms that the process is memoryless: it reacts to the current configuration of resources and needs without encoding past experience.

A similar pattern characterizes the hours of care not provided. Despite a slightly higher entropy rate ( $h_\mu \approx 1.9\text{--}2.3$ ), the process again reduces to a single causal state, indicating that variability is stochastic rather than structured. The introduction of a Hurdle–Gaussian Mixture symbolization slightly improved the descriptive fit, but the underlying informational structure remains negligible. In substantive terms, this measure captures short-term mismatches between caregiving capacity and demand—episodes that arise independently across simulation ticks rather than as part of a cumulative trajectory. The low  $C_\mu$  and minimal  $E_{\text{proxy}}$  thus reflect a process governed by cross-sectional heterogeneity rather than by endogenous feedback or adaptation.

By contrast, the walkability variable exhibits a markedly different informational signature. Under ordinal symbolic encoding (embedding dimension  $m = 3\text{--}4$ ), the reconstructed  $\varepsilon$ -machines reveal between 12 and 20 causal states, with complexity values in the range  $C_\mu \approx 3.3\text{--}3.6$  and positive predictive information ( $E_{\text{proxy}} = 0.3\text{--}1.2$ ). The entropy rate remains high but stable ( $h_\mu \approx 2.1\text{--}3.3$ ), indicating the coexistence of stochastic and deterministic elements. This configuration is typical of processes in which spatial continuity and behavioral feedback jointly generate structured but non-periodic dynamics. In this model, *walkability* synthesizes the influence of infrastructure, terrain, and service distribution with the movement routines of the dyads. As agents repeatedly interact with a constrained environment, localized accessibility patterns emerge, generating recurrent—though not fully deterministic—mobility regimes. The resulting  $\varepsilon$ -machine suggests a bounded but genuine temporal memory, in which present states retain information about prior accessibility conditions.

Taken together, these results delineate a clear distinction between static socioeconomic constraints and dynamic spatial interactions within the simulated caregiving environment. The first two variables (*efforts* and *hours not cared*) behave as conditionally independent draws shaped by exogenous attributes; the third (*walkability*) reflects an endogenous spatio-behavioral subsystem capable of storing and transmitting information across time. In informational terms, the caregiving process appears *structurally flat* in its socioeconomic dimension but *dynamically rich* in its spatial and mobility component. This finding supports the interpretation that infrastructural and environmental factors—rather than individual or household resources—constitute the principal carriers of systemic complexity and feedback in the simulated model of care accessibility.

From a methodological standpoint, the contrast among these variables illustrates the diagnostic value of  $\varepsilon$ -machine reconstruction for agent-based simulations. When applied to outputs derived from mixed socioeconomic and spatial processes, computational-mechanics metrics provide a compact representation of where and how information is stored in the system. In this case, the emergence of multiple causal states in *walkability* but not in *effort* or *care deficit* time series indicates that spatial interactions operate as the primary generator of temporal organization. Future extensions could explicitly couple these subsystems—for example, allowing caregiver fatigue or service accessibility to evolve as a function of prior overload or mobility episodes—to test whether feedback between socioeconomic and spatial dimensions increases the system’s overall statistical complexity and predictive capacity.

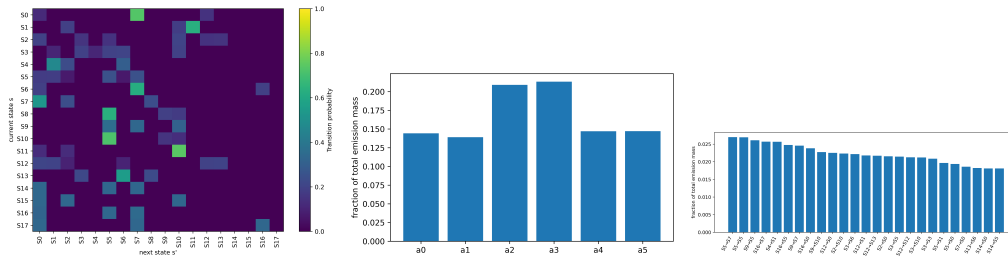


Figure 1: Structural signatures. Left: State–transition probability matrix. Heatmap of transition probabilities between causal states (rows = current  $s$ , columns = next  $s'$ ). Bright diagonal elements indicate persistence within the same state, whereas off-diagonal clusters denote systematic switching among subsets of states. The resulting pattern highlights modular organization and localized predictability within the global  $\varepsilon$ -machine. Emission and transition mass distributions. Middle: Fraction of total emission probability associated with each ordinal symbol ( $a_0$ – $a_5$ ). Middle-range motifs ( $a_2$ ,  $a_3$ ) dominate, suggesting gradual rather than abrupt changes in relative walkability. Right: Most probable state-to-state transitions (top 25 by mass). The concentration of probability mass among a few edges (e.g.,  $S_5 \rightarrow S_7$ ,  $S_5 \rightarrow S_5$ ) indicates limited recurrent micro-patterns and short-range stability.

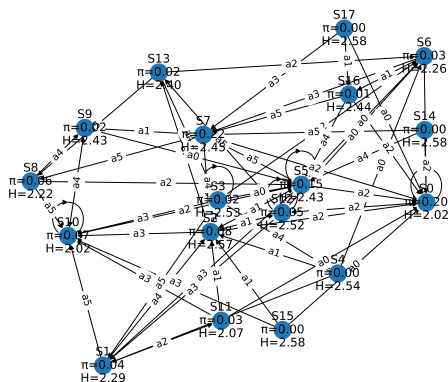


Figure 2: Global  $\varepsilon$ -machine for walkability (ordinal  $m = 3$ ). Directed graph representation of the reconstructed  $\varepsilon$ -machine. Nodes correspond to causal states ( $S_0$ – $S_{17}$ ) annotated with their stationary probability ( $\pi$ ) and local emission entropy ( $H$ ). Edges denote predictive transitions labeled by emitted ordinal symbols ( $a_0$ – $a_5$ ). The layout reveals a moderately connected topology with clusters of recurrent states and several self-loops, indicating locally stable yet globally fragmented dynamics.

The directed graph representation of the reconstructed  $\varepsilon$ -machine provides a visual summary of the system’s internal information architecture. Each node represents a *causal state*, labeled by its stationary probability ( $\pi$ ) and local emission entropy ( $H$ ), while directed edges encode transitions labeled by emitted ordinal symbols ( $a_0$ – $a_5$ ). The resulting topology captures how past configurations of the process are used to generate its future evolution. In the global  $\varepsilon$ -machine for *walkability* ( $m = 3$ ), the network exhibits a moderately connected structure with a limited number of high-probability nodes and recurrent loops. This pattern indicates that the system’s predictive organization is *localized*—information tends to circulate within small state clusters rather than propagate through long transition chains. Such a structure implies short-range predictability and context-bound adaptation rather than persistent global memory.

Complementary visualizations of the same  $\varepsilon$ -machine help to uncover additional layers of structure. The state–transition heatmap acts as a *structural signature* of the reconstructed process: each cell encodes the empirical probability of transitioning from state  $i$  to state  $j$  within either the global or per-dyad symbolic sequence.

- Diagonal dominance denotes *persistence*: agents or dyads tend to remain

in similar ordinal configurations across successive time steps, suggesting that local walkability (or caregiving effort) states are self-reinforcing.

- Off-diagonal clusters or bands reveal *systematic switching*, that is, recurring transitions between specific subsets of states, often corresponding to alternating behavioral or spatial regimes (e.g., shifts between high- and low-accessibility contexts or cyclical caregiving routines).

This two-dimensional compression of the full  $\varepsilon$ -machine makes nonlinear dependencies and *predictive symmetry* visually salient, facilitating cross-comparison of simulations under different contextual or policy conditions.

The symbol histogram summarizes the marginal distribution of ordinal patterns—here, the six motifs  $a_0$ – $a_5$  generated for  $m = 3$ . It effectively captures the *compositional balance* of local dynamics.

- A *flat* histogram signals near-equiprobable symbol usage, implying unstructured or noise-like fluctuations.
- Conversely, *skewed* or *multimodal* distributions indicate dominance of particular directional motifs (e.g., monotonic increases or decreases in walkability), exposing *asymmetric dynamical tendencies* in the system.

This representation also provides an empirical check on the entropy-rate estimates ( $h_\mu$ ): strongly uneven symbol frequencies should coincide with lower entropy and hence greater short-range predictability.

Finally, the state-pair histogram aggregates transitions between causal states rather than symbols. It functions as a *coarse projection* of the  $\varepsilon$ -machine graph, emphasizing which causal transitions dominate the overall process without displaying the entire network.

- High-probability self-loops identify stable, quasi-stationary behavioral regimes.
- Concentrated transitions between a few state pairs delineate a *low-dimensional predictive core*, where the system’s dynamics can be summarized by a small number of recurrent pathways.
- Dispersed transition weights, by contrast, indicate *context-dependent or weakly structured memory*, a finding consistent with the relatively low  $E_{\text{proxy}}$  values estimated for most dyads.

### 6.1.1. Interpretation

The reconstructed  $\varepsilon$ -machine for *walkability*, obtained under an ordinal encoding with embedding dimension  $m = 3$ , reveals a moderately complex yet sparsely connected predictive structure. The causal-state network contains eighteen recurrent states, most of which exhibit small stationary probabilities and moderate local emission entropy ( $\approx 2$ – $2.6$  bits). The configuration points to a process that is locally regular but globally weakly coupled: individual dyads experience recurrent short-term mobility patterns, whereas transitions among those regimes remain infrequent.

The symbol-level distributions further clarify the system’s organization. The predominance of middle-rank ordinal motifs ( $a_2, a_3$ ) indicates that, for most dyads, changes in walkability occur gradually rather than through abrupt jumps. Extreme orderings ( $a_0, a_5$ ) are comparatively rare, suggesting that accessibility fluctuates within a limited dynamic range. Similarly, the transition-mass histogram demonstrates that a small subset of causal-state transitions concentrates most of the emission probability, implying that the overall process revisits a few micro-configurations repeatedly. This pattern is consistent with short-range stationarity and the predominance of local feedback mechanisms within each dyad’s spatial context.

The transition heatmap provides an additional structural perspective. The visible diagonal dominance corresponds to persistence, meaning that once the process occupies a particular causal state, it tends to remain there for multiple steps. At the same time, a few off-diagonal bands reveal recurrent oscillations between paired states—an indication of cyclical local adjustments rather than long-term directional trends. Collectively, these features suggest that the walkability dynamics, as captured at the dyad time scale, are quasi-stationary: they display internal memory and organization but only within limited temporal and spatial neighborhoods.

From a broader perspective, this global  $\varepsilon$ -machine constitutes a structural signature of the underlying simulated process. The moderate number of states, the partial diagonal dominance of the transition matrix, and the concentration of symbolic mass in a few motifs together depict a system where adaptation and inertia coexist. Walkability patterns are thus better described as *locally persistent and self-referential* rather than globally predictive. Detectable memory likely emerges only after conditioning on slower or aggregated temporal structures—such as daily or weekly rhythms—or through multivariate coupling with mobility and caregiving variables.

## 6.2. *Per-Dyad / Per-Variable $\varepsilon$ -Machine Reconstruction with Kolmogorov-Style Complexity Proxies*

While the global model (pooled series, single  $\varepsilon$ -machine) summarizes the system-level informational architecture through  $(h_\mu, C_\mu, E)$  and provides a useful baseline—for instance,  $L = 0$  implies that the pooled process is approximately memoryless under the chosen symbolic resolution—the per-dyad models recover idiosyncratic predictive structures and variability across agents and variables, with algorithmic proxies offering an orthogonal view of compressibility. Together, these representations separate semantic organization (via the  $\varepsilon$ -machine: predictive causation and memory) from syntactic simplicity (via compression: description length), yielding a unified lens on emergence, adaptation, and heterogeneity in agent-based model dynamics.

### 6.2.1. *Compression-Based Diagnostics of Structural Complexity*

Compression metrics provide an interpretable and low-dimensional summary of emergent structure in the simulation. The joint examination of statistical and algorithmic compressibility enables one to distinguish randomness from organized variability, to classify processes by stability versus intermittency, and to assess redundancy among symbolic representations. Such compression-based diagnostics therefore complement the  $\varepsilon$ -machine analysis by linking symbolic dynamics to computable measures of order, offering a quantitative signature of systemic organization that can be tracked across scenarios or policy interventions.

Specifically, we quantify statistical and algorithmic regularities across simulated variables (*efforts*, *wkb*, *hrsncared*). These indices capture different aspects of informational organization: the LZ78 normalized complexity (`lz78_norm`) reflects statistical unpredictability based on substring diversity, while the LZMA, BZ2, and GZIP *bits-per-symbol* (`bps`) values estimate algorithmic compressibility—how efficiently sequences can be encoded under general-purpose compression schemes. Together, these measures offer a dual view of structural variability: one grounded in symbolic recurrence and the other in algorithmic redundancy.

Table 1: Descriptive statistics and informational metrics across configurations: sample size per dyad ( $n$ ), alphabet size ( $A$ ), selected Markov order ( $L$ ), number of causal states  $|S|$ , entropy rate  $h_\mu$ , statistical complexity  $C_\mu$ , excess-entropy proxy  $E$ , and compression-based measures (LZMA/BZ2/GZIP bits-per-symbol; normalized LZ78).

Variable	Symbolization	$\overline{h}_\mu$	$\overline{C}_\mu$	$\overline{E}_{\text{proxy}}$	LZ78 <sub>norm</sub>	LZMA (bps)	BZ2 (bps)	GZIP (bps)	Mode $L$	Median $ S $
efforts	value	1.15 ± 1.01	0.01 ± 0.12	0.00 ± 0.00	0.90 ± 0.42	2.13 ± 1.46	1.70 ± 1.23	1.50 ± 1.15	0	1
hrsncared	value	2.01 ± 0.43	0.00 ± 0.00	0.00 ± 0.00	1.16 ± 0.14	3.52 ± 0.39	2.67 ± 0.34	2.52 ± 0.31	0	1
overwhelmed	binary	0.03 ± 0.15	0.00 ± 0.00	0.00 ± 0.00	0.45 ± 0.20	0.51 ± 0.19	0.30 ± 0.22	0.20 ± 0.18	6	1
wkb	ordinal	2.34 ± 0.81	0.13 ± 0.45	0.03 ± 0.09	0.67 ± 0.15	2.55 ± 0.58	1.79 ± 0.41	2.03 ± 0.54	0	1

*Summary of  $\varepsilon$ -Machine and Kolmogorov Metrics.* Table 1 summarizes the main outcomes across value-binned and ordinal encodings and parameter variants. Most dyads exhibit limited short-range predictability unless temporal symbolization explicitly encodes ordinal relations.

Table 2: Symbolization choices and recovered edges by variable. Value-binned variables (*efforts*, *hrsncared*) use global quantile and hurdle schemes; *wkb* (walkability) adopts ordinal encodings ( $m=3$  or  $m=4$ ).

Variable	Edges (bin boundaries or descriptor)	Labels
efforts	[0.0, 0.03, 0.19, 0.8]	['q1', 'q2', 'q3', 'q4', 'q5']
hrsncared	[0.0, 1e-12, 0.08, 1.26, 3.13, 10.07]	['zero', 'pos_q1', 'pos_q2', 'pos_q3', 'pos_q4']
wkb		['ordinal_m=4 (alphabet=24)']
wkb		['ordinal_m=3 (alphabet=6)']

*Symbolization Schemes and Edges.* Table 2 details the discretization edges. The balance between granularity and parsimony governs the trade-off between entropy and over-segmentation.

Table 3: Model selection summary for ordinal walkability across dyads and merge thresholds. Conservative merging with  $m=4$  yields  $L=0$  for most dyads; reducing to  $m=3$  and relaxing merges reveals finite memory ( $L=1-2$ ) for a subset.

Statistic	# Dyads	Pr( $L > 0$ )	Pr(practical memory)	Mean $L \pm SD$
wkb (ordinal)	94	10.3%	8.2%	$0.21 \pm 0.90$

*Ordinal Walkability: Model Selection Across Dyads.* Table 3 shows that most dyads collapse to  $L=0$  under conservative merging, confirming weak short-range memory. With  $m=3$  and relaxed merging, a subset exhibits finite predictive structure ( $L=1-2$ ) and moderate excess entropy.

*Statistical vs. Algorithmic Compressibility.* The scatterplot of `lz78_norm` versus `lzma_bps` provides a two-dimensional projection of statistical and algorithmic complexity. Points aligned along the main diagonal denote sequences that are simultaneously complex in a statistical sense yet compressible algorithmically—structured but not trivially repetitive (frequent for *walkability* and *efforts*). Deviations from the diagonal, particularly **high `lzma_bps` with low `lz78_norm`**, indicate algorithmic irregularity: symbol sequences that lack local redundancy yet embed context-dependent transitions—typical of intermittent caregiving or fluctuating accessibility where abrupt changes dominate over persistent cycles.

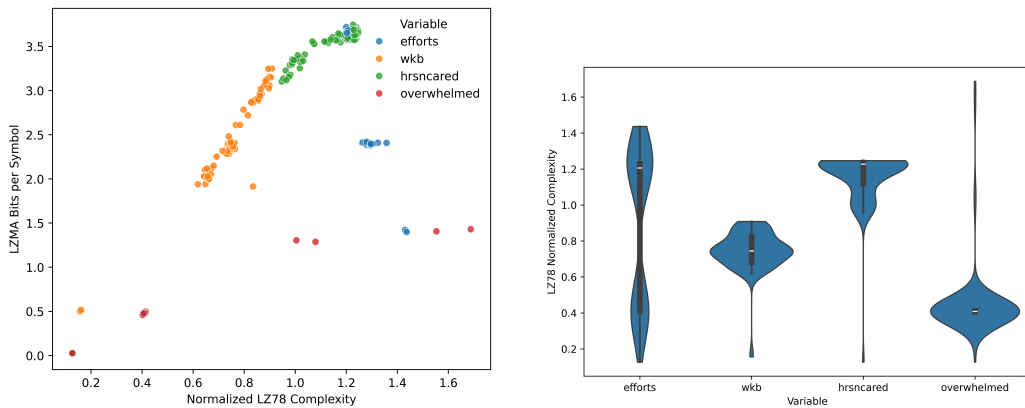


Figure 3: Left: normalized LZ78 complexity vs. LZMA bits per symbol (statistical vs. algorithmic compressibility). Right: violin plots of normalized LZ78 by variable showing heterogeneity and burstiness.

*Distributional Structure Across Variables.* Boxplots and violin plots of the compression metrics by variable illustrate distinct informational signatures. *Efforts* displays narrow and nearly symmetric distributions, indicating stable, low-variance dynamics consistent with short-range memoryless behavior. In contrast, *walkability (wkb)* and *hours not cared* exhibit broader and often asymmetric profiles, suggesting heterogeneous or bursty processes that reflect spatial and caregiving variability within the simulation. Overall, the behavioral and spatial dimensions differ in their intrinsic regularity, with *efforts* serving as a quasi-stationary reference and *wkb* capturing higher-order nonlinear variability.

*Correlations Among Compression Measures.* Table 4 reports pairwise correlations among the compression-based metrics (`lzma_bps`, `bz2_bps`, `gzip_bps`, and `lz78_norm`). The results show strong interdependence among dictionary compressors—LZMA, BZ2, and GZIP—(typically  $\rho > 0.9$ ), confirming that these algorithms provide consistent estimates of algorithmic compressibility. In contrast, the normalized LZ78 complexity diverges moderately ( $\rho \approx 0.7\text{--}0.8$ ), indicating that statistical and algorithmic compressibility capture complementary informational dimensions. Whereas compression ratios quantify encoding efficiency, normalized LZ78 reflects the rate of novel pattern introduction. High statistical complexity combined with moderate algorithmic compressibility typifies structured yet nonreducible dynamics, a hallmark of adaptive, path-dependent agent-based systems.

Table 4: Correlation matrix among compression metrics (LZ78, LZMA, BZ2, GZIP). High inter-algorithm correlations ( $> 0.9$ ) indicate redundancy among compressors, whereas moderate divergence from LZ78 suggests complementary sensitivity to symbolic recurrence.

	LZMA (bps)	BZ2 (bps)	GZIP (bps)	LZ78 <sub>norm</sub>
LZMA (bps)	1.00	0.98	0.99	0.85
BZ2 (bps)	0.98	1.00	0.98	0.90
GZIP (bps)	0.99	0.98	1.00	0.82
LZ78 <sub>norm</sub>	0.85	0.90	0.82	1.00

### 6.2.2. Interpretation

The plots jointly characterize the compressibility and structure of dyad-level time series, revealing how the informational content of each behavioral dimension (*efforts*, *walkability index [wkb]*, *hours not cared*, and *overwhelmed status*) differs when viewed through statistical versus algorithmic lenses.

Two main regimes emerge. The first corresponds to a diagonal band in the LZ78–LZMA scatterplots, where statistical and algorithmic compressibility are highly dependent. These sequences are structured yet predictable, indicating organized variability rather than noise. The second regime consists of outliers characterized by high `lzma_bps` but low `lz78_norm`, reflecting algorithmic irregularity driven by intermittent or context-dependent transitions. Variable-level clustering suggests that behavioral regularity and spatial accessibility interact differently with predictability, depending on whether dynamics are continuous, as in *efforts*, or episodic, as in *hours not cared*.

Normalized LZ78 distributions further differentiate the informational geometry of variables. The *efforts* and *hours not cared* series display higher medians and moderate dispersion, indicative of steady but nuanced dynamics. In contrast, *walkability* shows lower and narrower complexity, constrained by the ordinal structure of the spatial network, while the *overwhelmed* variable exhibits strong asymmetry and occasional multimodality consistent with threshold-type behavior.

Compression bits-per-symbol derived from LZMA, BZ2, and GZIP confirm these patterns. The wider dispersion observed for *efforts* and *walkability* signals heterogeneous temporal organization, whereas *hours not cared* exhibits narrower interquartile ranges, implying quasi-stationary dynamics once a caregiving rhythm stabilizes. The *overwhelmed* variable, in contrast, presents near-zero median values, reflecting a binary regime with minimal informational entropy.

Correlations among compression metrics reinforce this interpretation. Dictionary-based compressors (LZMA, BZ2, GZIP) show very high mutual dependence ( $\rho > 0.97$ ), indicating they capture overlapping redundancy structures, while their weaker association with normalized LZ78 ( $\rho \approx 0.7\text{--}0.8$ ) highlights the complementary nature of the two perspectives. Whereas dictionary compressors quantify algorithmic predictability through redundancy elimination, LZ78 emphasizes statistical recurrence and symbolic novelty. Considering both metrics thus provides a robust diagnostic framework for detecting the emergence of complexity and variability in agent-level behavioral trajectories.

Overall, the results indicate that most dyads exhibit moderate algorithmic structure rather than purely random or deterministic dynamics. Temporal heterogeneity varies systematically across behavioral variables, reflecting diverse cognitive and spatial constraints. Statistical and algorithmic measures, though correlated, are not interchangeable; together they offer a more com-

prehensive understanding of how predictability and adaptation emerge in the caregiving system.

## 7. Discussion, Limitations, and Conclusions

Compared with prior computational-mechanics studies that focus on theoretical or synthetic sources, the present framework operationalizes intrinsic computation in an applied, data-driven ABM setting, enabling systematic evaluation of informational dynamics in social simulations.

Methodologically, this study bridges theoretical computational mechanics and applied complexity analysis by embedding  $\varepsilon$ -machine reconstruction within an agent-based modeling workflow. The proposed methodology integrates symbolic dynamics, causal-state reconstruction, and algorithmic compressibility to evaluate informational organization in agent-based simulations. This multi-level representation—from symbol transitions to  $\varepsilon$ -machines and compression metrics—yields a reproducible and quantitative description of emergent predictability and structural heterogeneity in simulated social systems.

Whereas intrinsic computation traditionally quantifies how a stationary process stores and transmits information, our approach treats each dyad-level time series as a locally adaptive source whose causal states evolve under behavioral and spatial constraints. The addition of algorithmic-compression diagnostics extends this perspective beyond state entropy to measurable description length, providing a practical analogue of the system’s effective complexity. In this sense, the proposed approach translates the informational architecture emphasized by Shalizi and Crutchfield into a form suitable for empirical systems characterized by heterogeneity, nonstationarity, and feedback—hallmarks of complex adaptive social environments.

Across variables and symbolizations, results indicate that *efforts* and *hrsncared* behave as nearly memoryless processes at the dyad cadence, whereas ordinal *walkability* retains traces of structured but weak predictability. This suggests that short-range predictability remains limited unless (a) slower temporal baselines (e.g., hour-of-day, day-of-week, or mobility strata) are introduced, (b) embedding delays ( $\tau > 1$ ) capture slower geometric variations, or (c) multivariate  $\varepsilon$ -machines jointly model walkability, mobility, and caregiving context. We adopt an ordinal symbolization scheme that stabilizes predictive information without over-merging, recognizing that detectable memory likely emerges only after conditioning or at coarser temporal scales. Overall, the

results demonstrate that the joint use of  $\varepsilon$ -machines and compression-based diagnostics effectively separates *semantic organization* (predictive structure and causal memory) from *syntactic simplicity* (description length), providing a unified lens for examining emergence and adaptation in complex agent-based systems.

*Summary of Findings..* Coupling  $\varepsilon$ -machines with compression diagnostics yields a coherent picture of where predictive information resides in the caregiving ABM. Global reconstructions furnish a baseline (often  $L=0$  for pooled series under coarse symbolizations), while per-dyad models reveal localized structure, especially for *walkability* under ordinal encodings ( $m=3$ ). Compression results corroborate this: dictionary compressors agree strongly on algorithmic redundancy, whereas normalized LZ78 highlights statistical novelty via substring diversity.

*Interpretation..* Socioeconomic variables largely reflect cross-sectional heterogeneity, exhibiting near-memoryless dynamics at dyad cadence, while spatial interaction—encoded by *walkability*—induces bounded temporal memory and localized recurrent regimes. The contrast validates the joint diagnostic: *semantic organization* (predictive states and memory) is cleanly separated from *syntactic simplicity* (description length), clarifying how emergence manifests at different layers of the system.

*Methodological Implications..* Symbolization is not neutral: ordinal encodings preserve temporal geometry, and hybrid Hurdle–GMM captures zero inflation. Large alphabets ( $m=4$ ) can induce effective sparsity, hiding finite memory; moderate alphabets ( $m=3$ ) with calibrated merging recover it. We recommend reporting  $h_\mu/\log_2 A$ ,  $C_\mu$ , and  $E_{\text{proxy}}$  alongside compression bits-per-symbol and LZ78 indices to assess stability across symbolizations.

*Limitations and Robustness..* Reconstruction quality depends on symbolization, sequence length, and stationarity; short or highly entropic series can bias state estimates or collapse to trivial machines. We mitigate these issues through entropy-balanced or quantile binning, hurdle modeling for zero-inflated variables, BIC-based order selection, and complementary algorithmic proxies that retain discriminatory power when predictive structure is minimal. Possible extensions include ordinal-pattern symbolization, Bayesian smoothing of predictive distributions, and cohort pooling for short sequences.

*Future Directions.*.. Uncertainty quantification for  $(h_\mu, C_\mu, E_{\text{proxy}})$  and compressor-based indices should be added via block bootstrap or parametric surrogates. Future extensions include multivariate  $\varepsilon$ -machines (jointly modeling walkability, mobility, and caregiving context), delayed embeddings ( $\tau > 1$ ) for slower rhythms, and targeted symbolizations informed by control or policy levers. Extending this framework to interactive, nonstationary, or policy-driven ABMs could help bridge informational and causal perspectives on social complexity, consistent with current efforts to quantify emergence and adaptation in empirical complex systems.

## Funding

This work was supported by the European Union – Next Generation EU under the National Recovery and Resilience Plan (NRRP) project Age-It (AGE-IT – PE00000015; CUP: H43C22000840006).

## Data availability

All simulation code, parameter files, and processed datasets used in this study are available from the corresponding author upon reasonable request. The source code for symbolization,  $\varepsilon$ -machine reconstruction, and complexity proxies (normalized LZ78 and compression-based metrics) will be archived with a versioned hash to ensure reproducibility. The dataset schema includes identifiers (`id_caregiver`), temporal fields (`tick`, `day`, `hour`), and observables (`efforts`, `wkb`, `hrsncared`, `overwhelmed`). Exact bin edges, tolerance parameters, and the maximum history length  $L_{\text{max}}$  will be documented alongside aggregate results to facilitate verification and reuse.

## Acknowledgments

The simulator employed in this study was developed for research and experimental purposes in collaboration with municipal authorities. All data handling and processing comply with the General Data Protection Regulation (Regulation (EU) 2016/679) and the licensing conditions of the Italian National Institute of Statistics (ISTAT). The system is exempt from the provisions of the EU Artificial Intelligence Act (Regulation (EU) 2024/1689) under the research exemption and is not classified as medical-device software under Regulation (EU) 2017/745.

During manuscript preparation, the author used digital assistants (ChatGPT, OpenAI; Perplexity.ai, San Francisco, CA; and Publish or Perish, Harzing.com) solely for language refinement, LaTeX and code editing, literature retrieval, and bibliometric verification. The author reviewed and edited all generated content and assumes full responsibility for the final text and its scientific interpretations. No financial or material support, administrative assistance, or in-kind contributions were received beyond the software tools explicitly mentioned above.

## References

- [1] Holland, J.H. Complex adaptive systems. *Daedalus* **1992**, *121*(1), 17–30.
- [2] Bonabeau, J.-L. Agent-based modeling: Methods and techniques for simulating human systems. *Proc. Natl. Acad. Sci. U.S.A.* **2002**, *99*(Suppl. 3), 7280–7287. doi:10.1073/pnas.082080899.
- [3] Epstein, J.M.; Axtell, R. *Growing Artificial Societies: Social Science from the Bottom Up*; Brookings Institution Press/MIT Press: Washington, DC/Cambridge, MA, USA, 1996.
- [4] Miller, J.H.; Page, S.E. *Complex Adaptive Systems: An Introduction to Computational Models of Social Life*; Princeton University Press: Princeton, NJ, USA, 2007.
- [5] Holland, J.H. Studying complex adaptive systems. *J. Syst. Sci. Complex.* **2006**, *19*(1), 1–8.
- [6] Levin, S.A. Ecosystems and the biosphere as complex adaptive systems. *Ecosystems* **1998**, *1*(5), 431–436.
- [7] Levin, S.A. Exploring the known, the unknown, and the unknowable in complex systems. *Bull. Am. Math. Soc.* **2002**, *40*(1), 3–19. doi:10.1090/S0273-0979-02-00965-5.
- [8] Epstein, J.M. Agent-based computational models and generative social science. *Complexity* **1999**, *4*(5), 41–60.
- [9] Epstein, J.M. *Generative Social Science: Studies in Agent-Based Computational Modeling*; Princeton University Press: Princeton, NJ, USA, 2012.

- [10] Crutchfield, J.P.; Young, K. Inferring statistical complexity. *Phys. Rev. Lett.* **1989**, *63*(2), 105–108.
- [11] Crutchfield, J.P. The calculi of emergence: Computation, dynamics, and induction. *Physica D* **1994**, *75*(1–3), 11–54.
- [12] Shalizi, C.R.; Crutchfield, J.P. Computational mechanics: Pattern and prediction, structure and simplicity. *J. Stat. Phys.* **2001**, *104*(3–4), 817–879.
- [13] Cover, T.M.; Thomas, J.A. *Elements of Information Theory*, 2nd ed.; Wiley: Hoboken, NJ, USA, 2006.
- [14] Schwarz, G. Estimating the dimension of a model. *Ann. Stat.* **1978**, *6*(2), 461–464. doi:10.1214/aos/1176344136.
- [15] Jenks, G.F. The data model concept in statistical mapping. *Int. Yearb. Cartogr.* **1967**, *7*, 186–190.
- [16] Li, M.; Vitányi, P. *An Introduction to Kolmogorov Complexity and Its Applications*, 3rd ed.; Springer: New York, NY, USA, 2008. doi:10.1007/978-0-387-49820-2.